CIRP Journal of Manufacturing Science and Technology 37 (2022) 584–595

Contents lists available at ScienceDirect

CIRP Journal of Manufacturing Science and Technology

journal homepage: www.elsevier.com/locate/cirpj

Effect of the welding technique on mechanical properties and metallurgical characteristics of the naval grade high strength low alloy steel joints produced by SMAW and GMAW

P. Hariprasath[a,*], P. Sivaraj[a], V. Balasubramanian[a], Srinivas Pilli[b], K. Sridhar[b]

[a] Centre for Materials Joining and Research (CEMAJOR), Department of Manufacturing Engineering, Annamalai University, Annamalai Nagar 608002, India
[b] Naval Materials Research Laboratory (NMRL), Ambernath, Mumbai 421506, India

ARTICLE INFO

Available online 24 March 2022

Keywords:
High strength low alloy steel
Tensile strength
Microhardness
Microstructure

ABSTRACT

Naval grade, high strength low alloy (HSLA) steel is designed especially for shipbuilding applications due to its high strength to weight ratio. The conventional fusion welding processes of shielded metal arc welding (SMAW) and gas metal arc welding (GMAW) are employed widely for structural applications. This work reports the influence of welding processes on mechanical properties and metallurgical characteristics of fusion welded DMR249A grade steel. The evaluating tensile, impact, microhardness properties were correlated with microstructures. The maximum recorded transverse tensile strength value of SMAW and GMAW joints were 558 MPa and 578 MPa. The lower microhardness had obtained in the subcritical heat-affected zone than other regions. The weld zone microstructure consists of fine, elongated, and columnar grain structures. From this investigation, it has been concluded that GMAW joints displayed marginally better properties than SMAW joints. But most weld failures has been observed in the subcritical heat-affected region; due to grain deformation and subsequent softening in the weldment.

© 2022 CIRP.

Introduction

High strength low alloy (HSLA) steel, were primarily developed to replace low-carbon steels in structural applications to improve the strength-to-weight ratio. DMR249A grade steel is a third-generation micro-alloyed low carbon steel and standardized grade for the construction of warships. This naval grade steel has compatible properties of high strength and resilience qualities; it is mainly due to alloying elements in the steel matrix [1,2]. And, these steel grades were susceptible to heat-affected zone failure such as cold cracking, which is eliminated by low hydrogen ferrite filler/electrode [3,4]. In general, the conventional fusion welding processes of shielded metal arc welding and gas metal arc welding had used in the construction of bridges, nuclear reactors, ships, and various machinery, because of the cost-effective and easy availability of processes [5–9]. Alipoor-amirabad et al. discussed the residual stress behavior and mechanical properties of micro-alloyed steel. The higher level of residual stresses is related to microstructural changes in weldment and HAZ regions [10]. Mao et al. reported the effect of nickel content on multipass welding of bainitic steel joints. The increasing Ni percentage changes the granular bainite to lath bainite or martensite in the weldment [11]. Lan et al. analyze the microstructural influence on the toughness property of submerged arc welded HSLA steel joints. They found dispersion of inclusion and their size cause the deterioration of HAZ toughness. The fusion zone had acicular ferrite morphology irrespective of heat input, though the size of the ferrite laths increased with heat input [12]. Jorge et al. reported the welding procedure and impact of post-weld heat-treated weld joints. A longer cooling time was tendencies to improve the toughness properties and reduction in mechanical properties of weldment [13]. Ragu Nathan and Balasubramanian et al. detailed the effect of welding processes on micro-alloyed steel. They studied the characteristics of the solid-state welding process over conventional fusion welding processes [14]. The above literature reported mechanical properties of various high-strength steels, but scanty research work on Naval base applications. Therefore, the welding of naval-based structural steels required more attention on shipbuilding applications. Hence, this study details the effect of fusion welding processes on mechanical properties and metallurgical characteristics of naval grade steel joints.

* Corresponding author.
E-mail addresses: hariprasathp12mech@gmail.com (P. Hariprasath), cemajorsiva@gmail.com (P. Sivaraj), visvabalu@yahoo.com (V. Balasubramanian), pillis.nmrl@gov.in (S. Pilli), sridsudi@gmail.com (K. Sridhar).

https://doi.org/10.1016/j.cirpj.2022.03.007
1755-5817/© 2022 CIRP.

Materials and methods

The rolled Naval grade HSLA steel with a thickness of 13 mm had acquired for this investigation. The chemical composition and mechanical properties of base metal and filler metals as shown in Tables 1 and 2. Fig. 1 presented the base metal microstructure of naval grade steel, which comprises 95% ferrite and 5% pearlite. The microalloying elements assist the superior material properties and relevant microstructures.

For joining, a single "V" (60°) notch is prepared with dimensions of 150 × 150 × 13 mm. Further, the rust and tissues were cleaned to avoid hot, cold cracking issues or foreign particle inclusion. The welding experiment was carry-out through a typical manual metal arc welding and gas metal arc welding. The consumables used for this investigation were E8018 – G and ER80s. Fig. 2a and b represented the joint configuration and fabricated SMAW and GMAW joints. Table 3 illustrates the welding parameters of root and capping passes. The fabricated joints have undergone into X-ray radiography test to qualify the defect-free sound weld. Then, the specimen extraction and corresponding ASTM standard specifications as shown in Fig. 2c and d. The transverse tensile test had conducted through a servomotor-enabled semi-automatic UTM machine with a capacity of 1000 kN. And, the impact toughness test had carried out using a manually controlled impact testing machine with a capacity of 300 J. The hardness measurement had performed using a Vickers microhardness testing machine with tentative conditions of 0.5 kg load and 15 s dwell time. Then, the welded coupons were cross-sectioned to evaluate the weld quality and characteristics using stereo zoom macroscopy and optical microscopy. The cross-sectioned metal coupon was mounted and mirror-polished using ultrafine grain diamond paste. And, the polished specimen was etched with freshly prepared Nital with a dwell time of 30–60 s. Subsequently, the fracture morphology had analyzed through scanning electron microscopy to reveal the mode of failure in welded joints. The evaluation of phase and elemental compositions using Energy Dispersive Spectroscopy (EDS) and X-ray diffraction (XRD) technique.

Results

Macrostructure

The macrostructure had used to examine visual defects and differentiate the various regions in the weldment. Fig. 3 presents the macrostructure of SMAW and GMAW joints, the different zones in the cross-section were weld metal zone (WM), coarse grain heat-affected zone (CGHAZ), fine grain heat-affected zone (FGHAZ), and base metal (BM). The thick steel plates joined with complete penetration and without any welding defects. While multi-pass welding, the bottom layer is greatly affected by heat during subsequent welding passes. It directly affects the weld quality and joint integrity [15]. Among the fusion weld, the bead geometrical changes occurred due to the heat input of the fusion welding processes. The bead width and weld metal area for the SMAW and GMAW joints were 27 mm, 29 mm, and 160 mm^2, 171 mm^2, which is evident in Table 4.

Tensile and impact toughness properties

The transverse tensile test had conducted in the welded joint as per the ASTM standard. The maximum recorded yield strength and

Table 1
Chemical composition (wt%) of Base metal and Filler metal.

Elements	C	Mn	Cr	N	Si	Mo	Ti	V	Nb	Ni	Cu	Al	Co	Fe	CE
DMR 249A	0.099	1.45	0.03	0.02	0.21	0.001	0.03	0.04	0.04	0.71	0.18	0.03	0.001	bal	0.44
E8018-G	0.08	1.4	0.01	0.009	0.2	0.15	0.02	0.01	0.02	2.3	0.05	0.015	–	bal	0.41
ER80S	0.08	1.3	0.02	0.008	0.3	0.17	0.01	0.02	0.023	2.8	0.035	0.014	–	bal	0.45

Table 2
Mechanical properties of Base metal and Filler metal.

S.No	0.2%Yield strength (MPa)	Ultimate Tensile strength (MPa)	Elongation in 50 mm gauge length (%)	Notch Tensile strength (MPa)	Notch strength Ratio (NSR)	Impact strength at RT (J)	Vickers hardness at 0.5 kg load (HV)
DMR 249A	485	614	28	654	1.05	208	273
E8018-G	521	625	22	–	–	190	290
ER80S	515	620	21	–	–	195	293

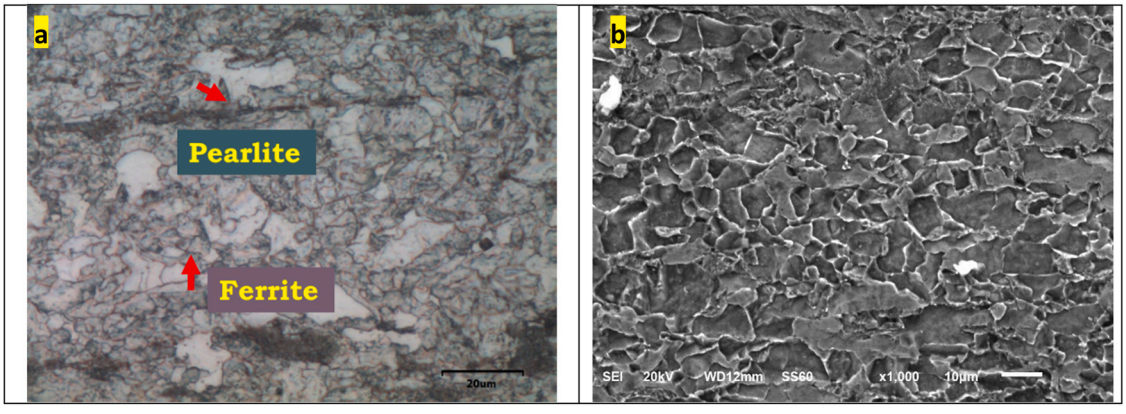


Fig. 1. (a-b). Microstructure of DMR249A grade steel.

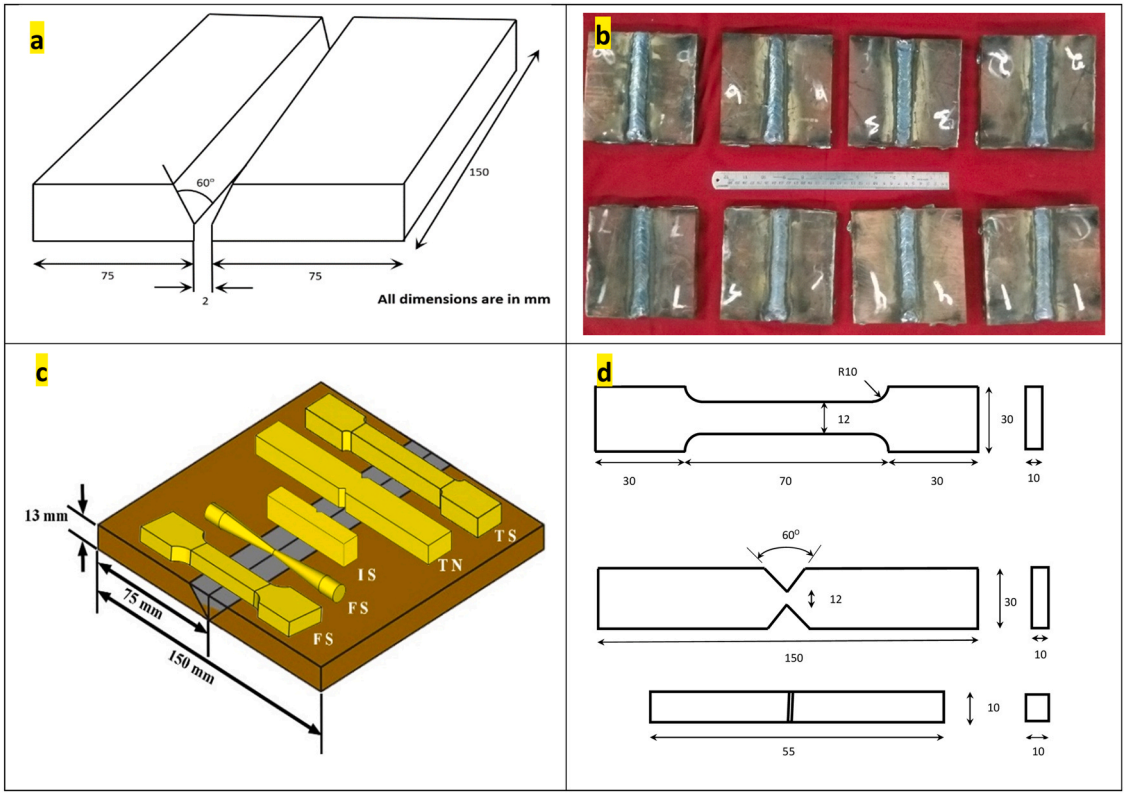


Fig. 2. (a) Joint configuration; (b) Fabricated SMAW & GMAW joints; (c) Specimen extraction diagram; (d) Dimension of notched, unnotched tensile & Impact specimens.

Table 3
Welding parameters and conditions used to fabricate the joints.

Welding Parameters	SMAW		GMAW	
	Root Pass	Capping Pass	Root Pass	Capping Pass
Filler metal	**E 8018G-C1**	**E 8018G-C1**	**ER80s**	**ER80s**
Filler diameter/mm	3.2	4	1.2	1.2
Pre-heating Temperature ℃	100	100	100	100
Inter pass Temperature ℃	125	125	125	125
Current/A	110	165	155	195
Voltage/V	21	27.5	22	29
Welding speed/(mm/min)	145	153	160	170
Heat input/(kJ/mm)	1.066		1.278	
No.of Passes (Include Caping)	6		5	

ultimate tensile strength of SMAW and GMAW joints were 473 & 480 MPa and 558 & 570 MPa. Fig. 4 illiterates the stress to displacement curve for both welded joints. While tensile testing, most of the weld failure occurred sub-critical interface region. It is mainly due to the formation of soft zones in the transition region [16]. From experimental results, the ductile mode of failure was observed from both weld joints and confirmed with the Notch strength ratio (NSR) higher than the unity value [17]. Fig. 5(a and b) presented the photograph of before and after tensile tested samples. Also, the impact toughness test was performed for welded joints and recorded maximum impact energy of 174 J & 178 J, as shown in Table 5. The prescribed table values are mean strength values by the average of three test results. The impact test samples evident ductility of the fusion weld joint, as shown in Fig. 5(c and d).

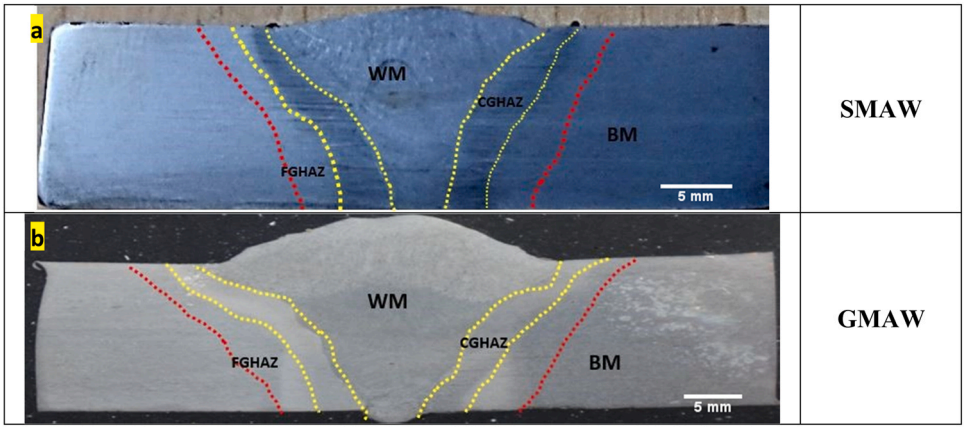


Fig. 3. Macrostructure of SMAW and GMAW joints.

Table 4
Bead Geometry analysis on SMAW and GMAW joints.

weld	Width of bead (mm)	Penetration (mm)	Weld metal area (mm^2)	HAZ area (mm^2)	Average width of the HAZ (mm)	Number of passes	Heat input (kJ/mm)
SMAW	27	12.4	160	60	4.5	6	1.066
GMAW	29	12.2	171	68	5	5	1.278

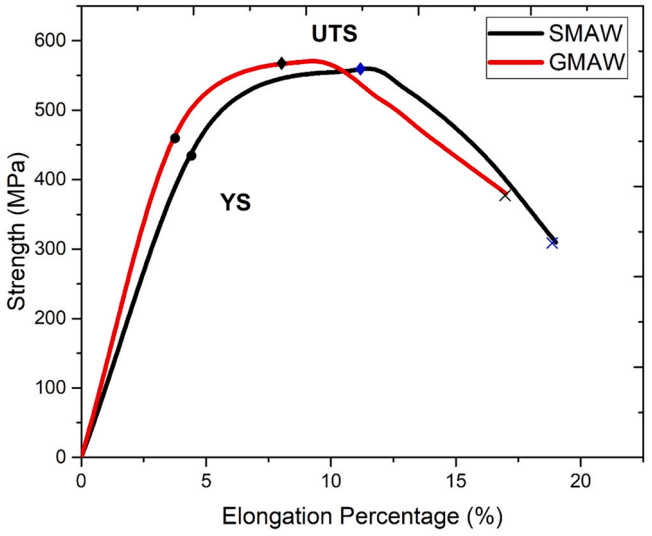


Fig. 4. Stress to Displacement curve for SMAW and GMAW.

Microhardness

The microhardness survey across the various zones of SMAW and GMAW joints had executed. The hardness value of weld metal typically varies with parent metal based on the heat dissipation rate from the weld center [18]. Fig. 6 presents the hardness map of the various region (FZ, CGHAZ, FGHAZ, and BM) and corresponding hardness values for the welded joints. The recrystallized weld zone had a hardness of 310 HV and 285 HV for GMAW and SMAW joints. Both fusion weld joints recorded maximum microhardness of 475 HV (GMAW) & 463 (SMAW) in the coarser grain heat-affected region. Then, the hardness drop occurred in the subsequent heat-affected zone. The lowest hardness was obtained in the sub-critical HAZ or HAZ to parent metal interface [19]. These softened regions reason for lower microhardness lends weld failure in both fusion-welded joints.

Microstructure

The microscopy study is a privileged tool to evaluate the metallurgical characteristics of the fusion-welded SMAW and GMAW



Fig. 5. (a-b). Before and After test of Smooth and Notch Tensile specimen; (c-d). Before and After test of Impact specimen.

Table 5
Tensile and Impact properties of SMAW and GMAW joints.

Joints	Yield strength (MPa)	Ultimate Tensile strength (MPa)	Elongation (%)	Notch Tensile strength (MPa)	Notch strength Ratio (NSR)	Impact strength at RT (J)	Vickers hardness at WM 0.5 kg load (HV)	Joint Efficiency (%)	Failure location
SMAW	473	558	19	578	1.03	174	304	88	**HAZ - BM interface**
GMAW	480	570	17	585	1.04	178	307	92	**HAZ - BM interface**

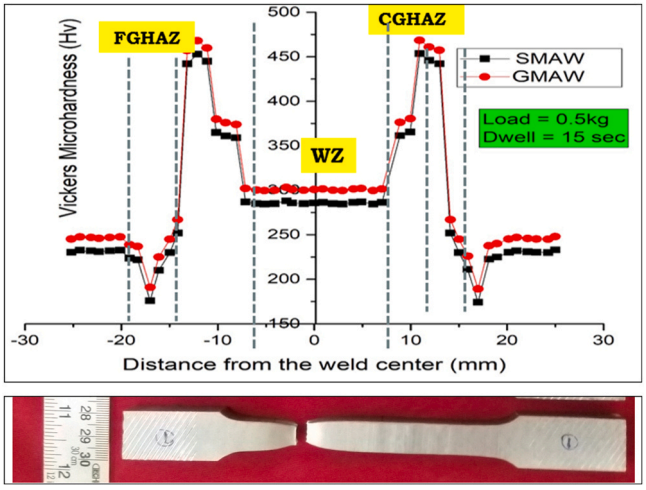


Fig. 6. Microhardness measurement across the mid thickness.

joints. The weld metal microstructure had composed of equiaxed grains at bottom layers and elongated columnar grains at top layers (Figs. 7a and 8a). The color-false microstructure (Figs. 7 and 8) had used to differentiate the phases in the weld cross-section [20]. The fusion zone having microstructure of pearlite, bainite, Widmanstädten and acicular ferrite phases in the steel matrix [21]. The SEM microstructure confirms the presence of upper and lower bainite in the fusion zone, which showed in Fig. 9. Fig. 10(a and b) illustrates that lath type upper bainite structure in the higher magnification TEM microstructure. Then, the coarser grain HAZ consists of bainite and acicular ferrite microstructure, as shown in Figs. 7b and 8b. The plastic strain and heat dissipation was the reason for the formation of coarser grains in the HAZ region. The segregation of alloying elements from the weld interface leads to hard bainite phases growth. Figs. 7c and 8c revealed FGHAZ, which had finer grains and a mixture of ferrite and pearlite phases. The FGHAZ impact of elastic distortion is minimal, so the hardness value is nominally higher than the base metal. Figs. 7d and 8d show the subcritical region or interface zone between the HAZ to the parent metal. The weld failure associated with these regions with a combination of lower hardness and polygonal ferrite microstructure [22].

Elemental and phase composition analysis

The elemental analysis is evidence for confirming chemical composition in the fusion-welded joints. The fusion zone microstructure of SMAW and GMAW had used for this investigation. Fig. 11 represents the EDS analyzed area, and corresponding elements were Fe, Ni, Cu, Si in the welded region. From this Elemental pattern, the iron and Nickel elements had dominant on both welded joints [23]. Further, the X-ray diffraction analysis brings about to determine the phase compositions. The XRD patterns were computed in the form of diffracted angle (2θ) to intensities (I/I0), as shown in Fig. 12. From the experimental results, the joint committee on diffraction standards confirms the presence of α-Fe, iron carbide (FeC), Fe-Ni, and Fe-Mn phases in both SMAW and GMAW weld cross-sections. The recorded diffraction angle and relative intensities for the welded joints were 45.22° (1000), 65.46° (346) for SMAW, and 42° (750), 48° (300), 73° (70), 88° (110), and 93° (60) for GMAW. And, the diffraction indices and corresponding d-spacing values of SMAW [101] 2.00520 Å, and [200] 1.42582 Å and GMAW [111] 2.0871 Å, [200] 1.8075 Å, [202] 1.2781 Å, [311] 1.0901 Å & [222] 1.0436 Å. Thus, the crystallinity patterns had evaluated from the selective area diffraction patterns. The observed Miller indices are [101], [200] and [111], [201] for the SMAW and GMAW joints, as shown in Fig. 10(c and d).

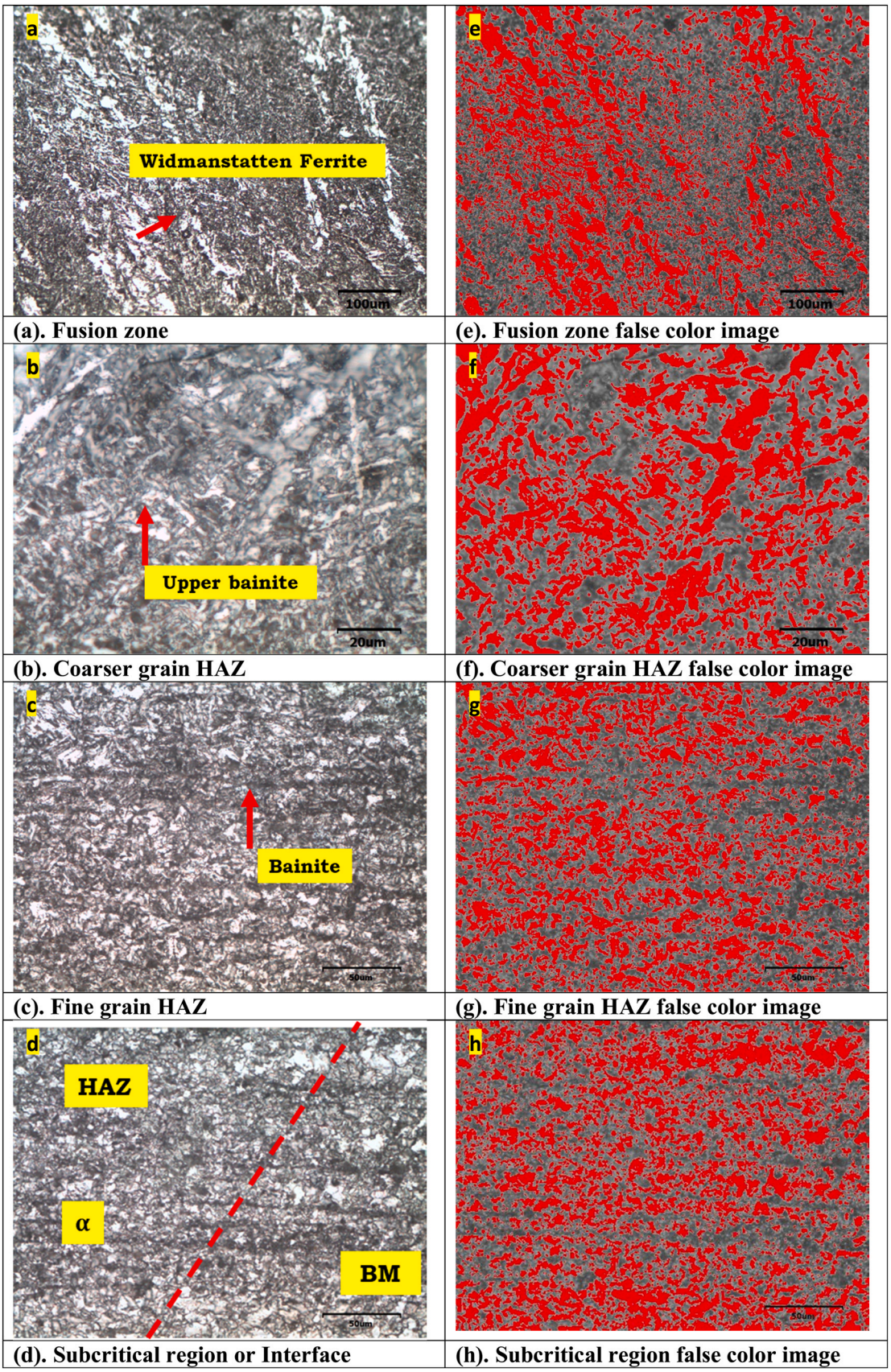


Fig. 7. Microstructure of SMAW joints (a) Fusion zone; (b) Coarser grain HAZ; (c) Fine grain HAZ; (d) Subcritical region or Interface; (e-h) color false microstructures.

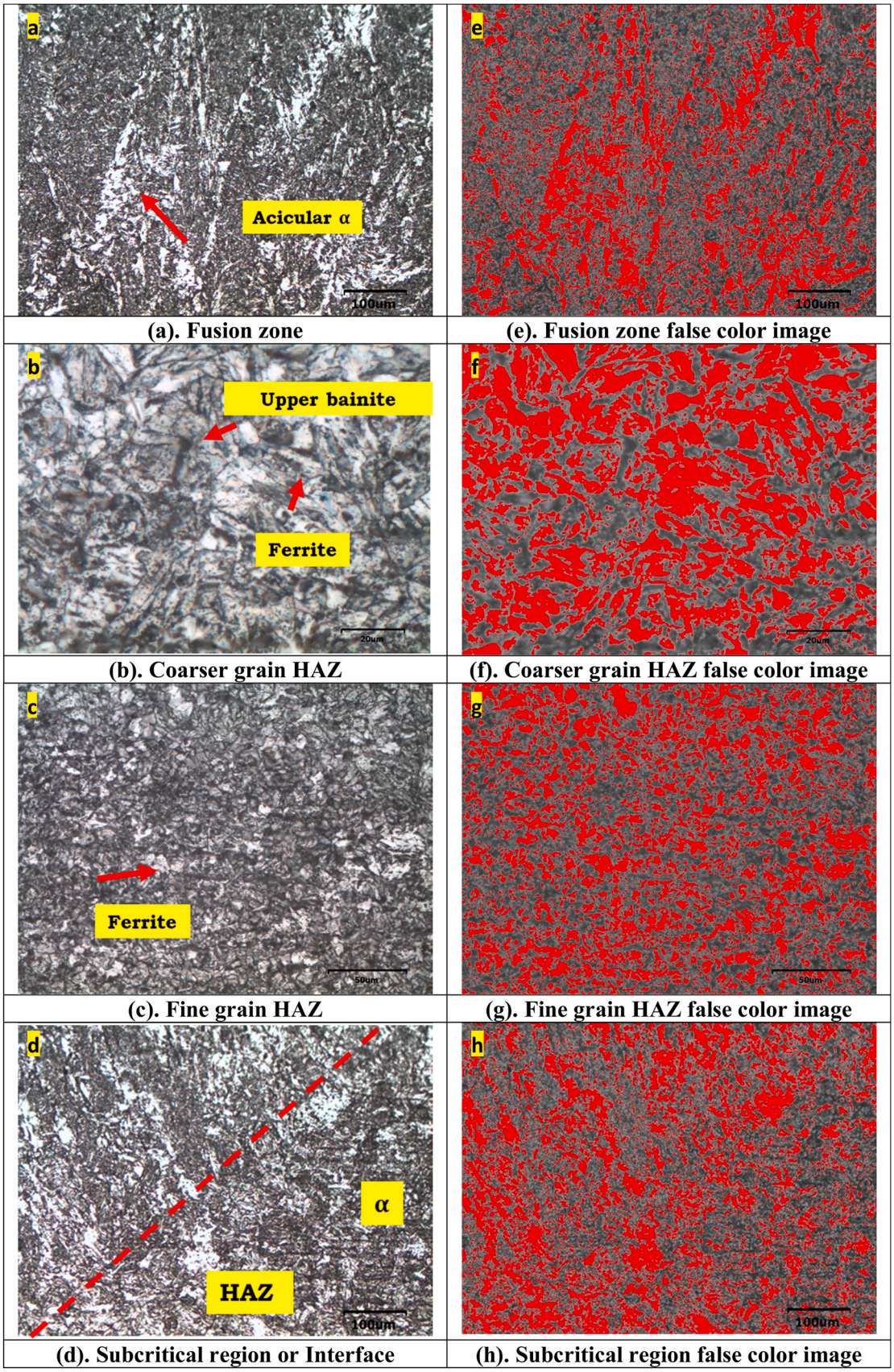


Fig. 8. Microstructure of GMAW joints (a) Fusion zone; (b) Coarser grain HAZ; (c) Fine grain HAZ; (d) Subcritical region or Interface; (e-h) color false microstructures.

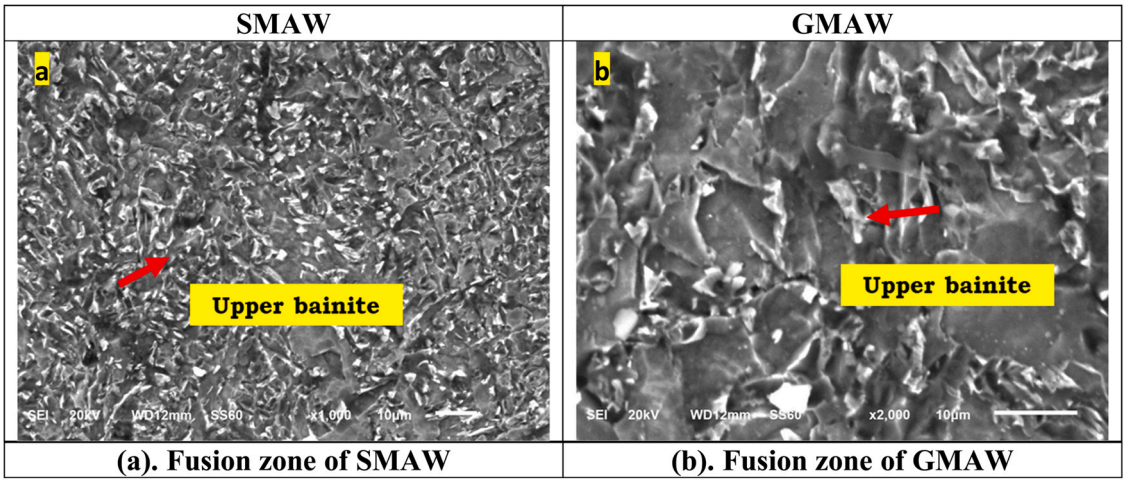


Fig. 9. SEM Microstructure of SMAW and GMAW joints.

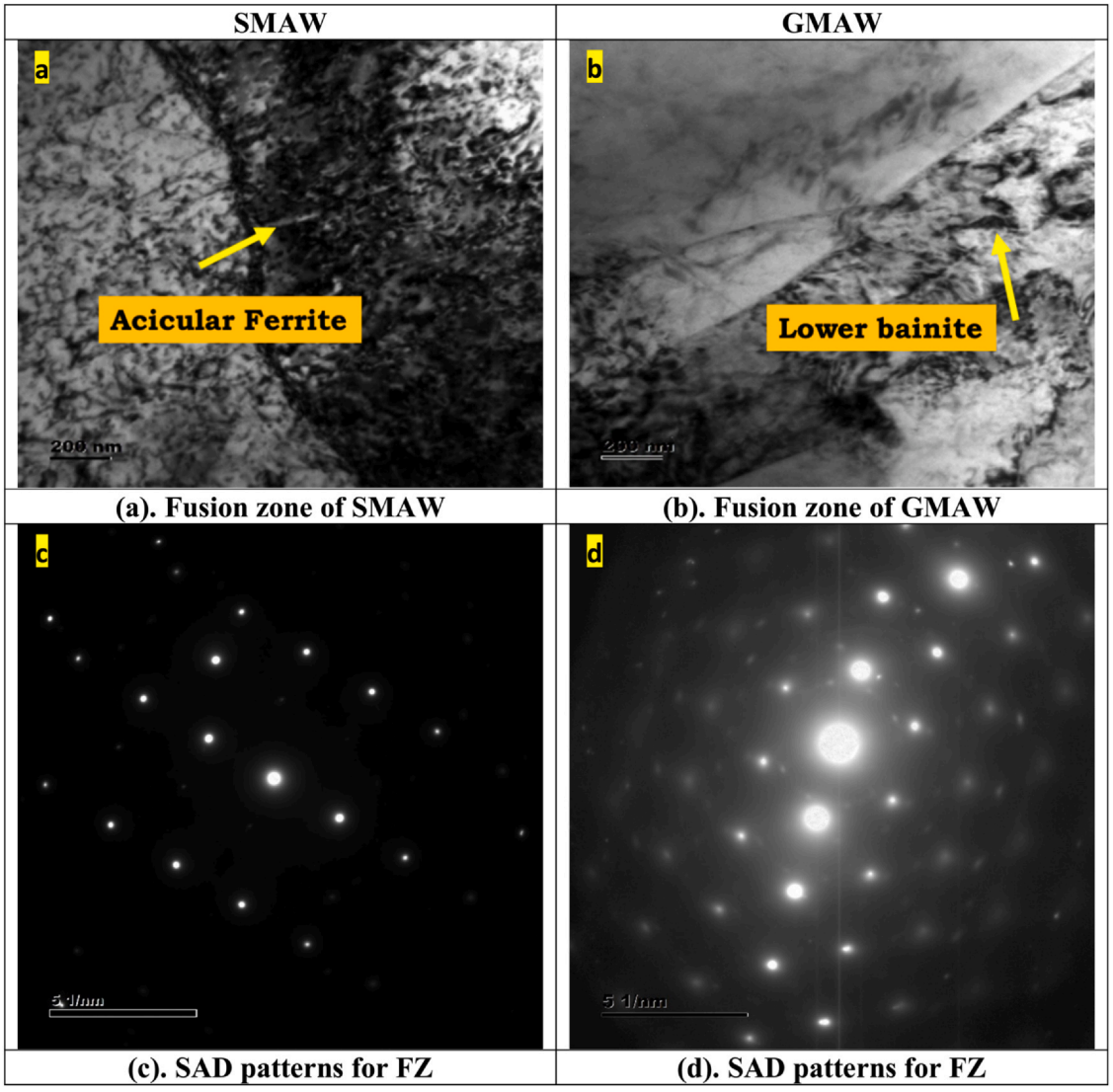


Fig. 10. TEM Microstructure of SMAW and GMAW joints.

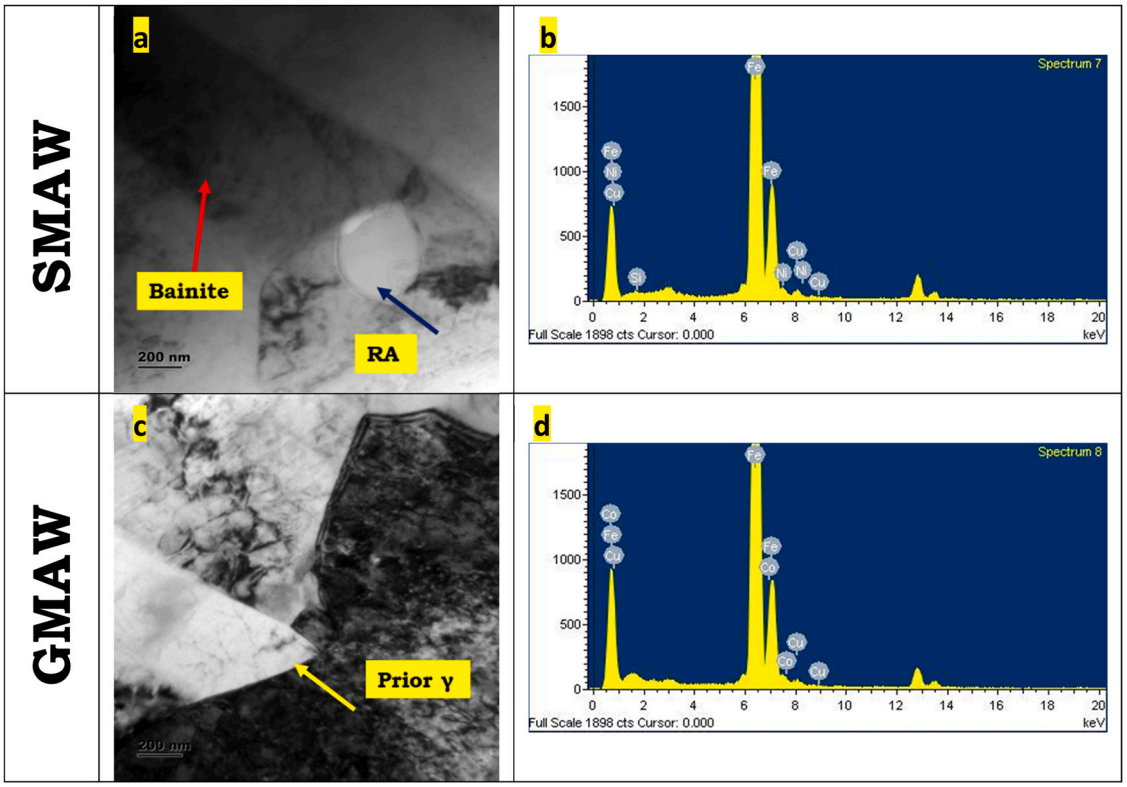


Fig. 11. Elemental analysis on interface region.

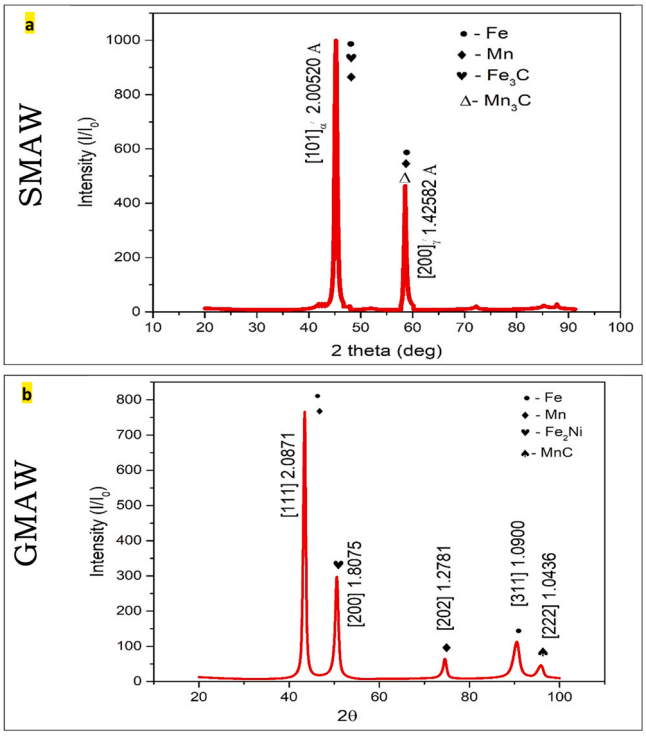


Fig. 12. X-ray diffraction patterns for SMAW and GMAW joints.

Fractography analysis

The fractography helps to reveal the mode of failure in the welded joints. The weld failure occurred in the subcritical HAZ region. Mostly, the weld failure had unveiled as a ductile fracture through the cup and cone features. Fig. 13(a and b) presents the large populations of dimple features in the propagation region of unnotched tensile specimens. The fibrous morphology is a measuring index for the ductility nature. The size of the dimples directly influences the mechanical properties of weldment [24]. Fig. 13(c and d) shows the fractography of the notched tensile specimen; it consists of dimples and microvoids features. Further, the fractography of the impact toughness specimen has composed of dimple features and wave marks, as shown in Fig. 14. The dimple feature is evident for significant toughness in both welded joints [25].

Discussion

The fusion welding of next-generation naval grade steel used for fabrication of hull structure in shipbuilding applications. From the experimental results, the visual examination (macrostructure) encounters common welding problems were porosity, undercut, and cold embrittlement [26]. The macrostructure analysis confirms the defect-free sound weld for both welded joints. And the bead geometry helps to quantify the fusion and HAZ region area followed by total heat input for the SMAW and GMAW joints [27]. The maximum obtained yield strength and tensile strength were 473 MPa, 558 MPa for SMAW & 480 MPa, 570 MPa for GMAW joints. The recorded joint efficiency of the weld joint is about 88% and 92% equal to the base metal. Mostly, the weld failure occurred in the HAZ interface region; it is mainly due to grain deformation followed by microstructure tempering [28]. The impact strength properties recorded a maximum of 174 J and 178 J due to microalloying elements in the naval steel. The microhardness graph exhibited hardness variation across the weld cross-section. And the microhardness evident that the subcritical region is a hardness dropping zone [29]. The fusion zone microstructure consists of acicular ferrite, pearlite, and bainite phases in the steel matrix, these phases are associated with Guo et al. [30]. The morphologies of these phases confirm with the corresponding color false image. The coarse grain heat-affected region is composed of bainite and acicular ferrite phases. The hard bainite

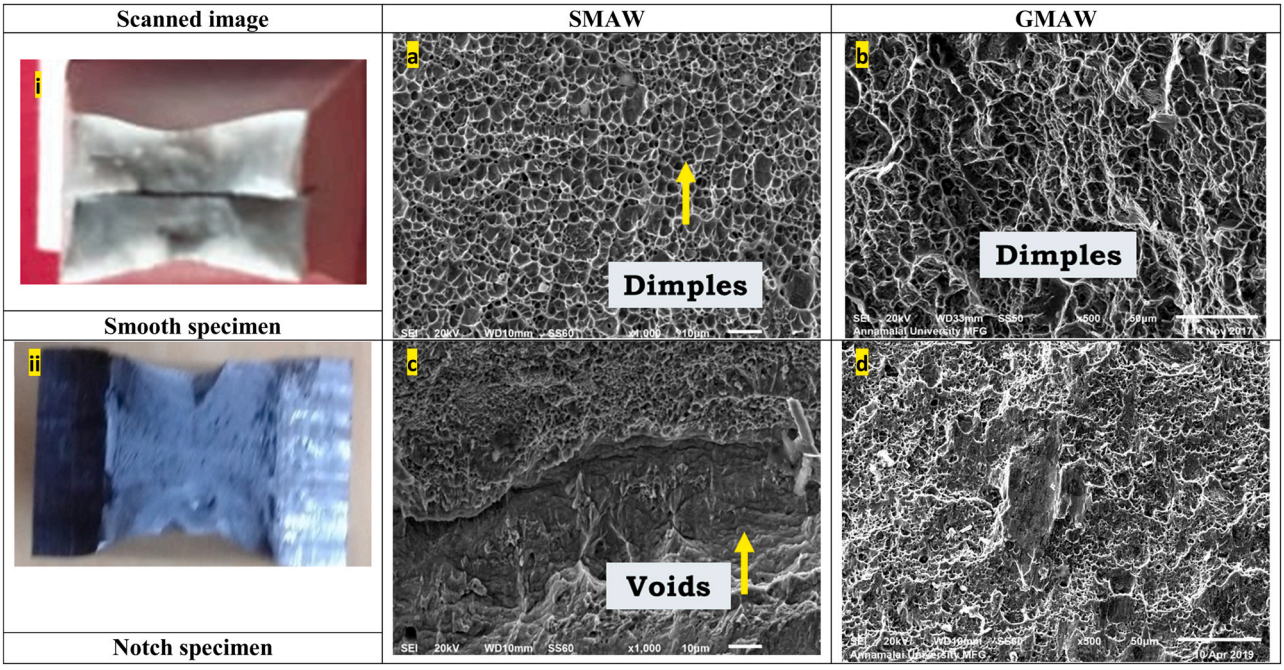


Fig. 13. SEM fractography of Smooth and Notch tensile specimens.

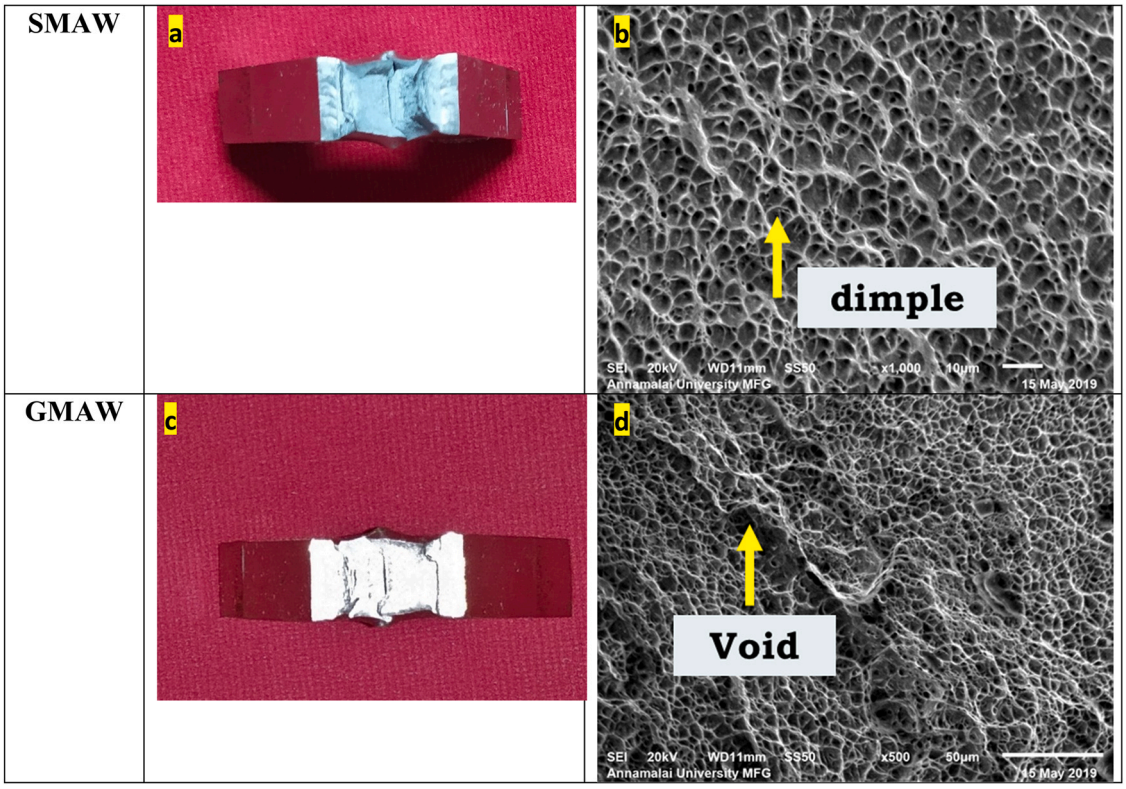


Fig. 14. SEM fractography of Impact specimens.

phases recorded superior microhardness. Further, the hardness dropping occurred severe heat dissipation leads to weld softening in the subcritical interface region. The bainite morphology is evident with the high magnification SEM and TEM microstructure [31]. The EDS analysis governs that elements in the fusion region were Fe, Ni, Cu, Co, Si; it evident with base metal and filler metal compositions. The phase composition identifies through XRD patterns and governs the metallic precipitates and intermetallic (Fe_2Ni, FeC, Fe_2C_3, and FeMn) from the weld section [32]. From this XRD patterns diffraction indices found to be [101] 2.00520 Å, and [200] 1.42582 Å for SMAW and [111] 2.0871 Å, [200] 1.8075 Å, [202] 1.2781 Å, [311] 1.0901 Å & [222] 1.0436 Å for GMAW. Although, the crystallinity studies of selective area diffraction patterns confirm the similar diffraction patterns of XRD analysis. The fractography resembles the ductile mode of failure that occurred in both SMAW and GMAW joints. The fracture surface contained a large number of fine dimple features along

with tiny voids [33]. Similarly, the impact samples fractography confirmed the ductility nature of weld joints.

Conclusion

From this investigation, the following conclusions derived

- The maximum recorded (0.2%) yield strength and ultimate tensile strength of the welded joints (SMAW & GMAW) were 473 MPa, 480 MPa, and 558 MPa, 570 MPa. The recorded impact toughness of 174 J, 178 J from SMAW and GMAW joints.
- The lower microhardness recorded in the interfacial region about 200 HV (SMAW), which lends to weld failure.
- The weld metal microstructure is composed of equiaxed grains at the bottom layers and elongated columnar grains at the top layers. And, the fusion zone having microstructure of pearlite, bainite, Widmanstädten and acicular ferrite phases in the steel matrix.
- The high magnification TEM images reveal the presence of bainite morphologies in the fusion zone.
- Most of the joints, the failure occurred at subcritical HAZ, which is due to elastic strain and distortion in the heat-affected region. The ductile mode of failure had observed during the tensile test.
- The EDS analysis governs the elements in the fusion region were Fe, Ni, Cu, Co, Si; it evident with base metal and filler metal composition. The phase composition identifies through Diffraction patterns; it governs the metallic precipitates and intermetallic (Fe_2Ni, FeC, Fe_2C_3, and Fe-Mn) from the weld section.
- The selective area diffraction patterns governed the crystallinity of both a fusion-welded joint, which is relative to XRD patterns.

Declaration of Competing Interest

The authors declare that they have no known competing financial interests or personal relationships that could have appeared to influence the work reported in this paper.

Acknowledgements

The authors express gratitude to the Director, Naval Research Board (NRB-DRDO), New Delhi, India for the financial support rendered through R & D project (Project number: NRB-443/MAT/18-19). And, the authors thanks to Naval Materials Research Laboratory (NMRL-DRDO), Mumbai, India for providing base materials to carry out this investigation.

References

[1] Caballero, F.G., Bhadeshia, H.K.D.H., Mawella, K.J.A., Jones, D.G., Brown, P., 2001, Design of Novel High Strength Bainitic Steels: Part 1. Materials Science and Technology, 17/5: 512–516. https://doi.org/10.1179/026708301101510348.
[2] Bose-Filho, W.W., Carvalho, A.L.M., Strangwood, M., 2007, Effects of Alloying Elements on the Microstructure and Inclusion Formation in HSLA Multipass Welds. Materials Characterization, 58/1: 29–39. https://doi.org/10.1016/J.MATCHAR.2006.03.004.
[3] Magudeeswaran, G., Balasubramanian, V., Reddy, G.M., Balasubramanian, T.S., 2008, Effect of Welding Processes and Consumables on Tensile and Impact Properties of High Strength Quenched and Tempered Steel Joints. Journal of Iron and Steel Research International, 15/6: 87–94. https://doi.org/10.1016/S1006-706X(08)60273-3.
[4] Lan, H.F., Du, L.X., Li, Q., Qiu, C.L., Li, J.P., Misra, R.D.K., 2017, Improvement of Strength-toughness Combination in Austempered Low Carbon Bainitic Steel: The Key Role of Refining Prior Austenite Grain Size. Journal of Alloys and Compounds, 710:702–710. https://doi.org/10.1016/J.JALLCOM.2017.03.024.
[5] Khurshid, M., Barsoum, Z., Mumtaz, N.A., 2012, Ultimate Strength and Failure Modes for Fillet Welds in High Strength Steels. Materials & Design, 40:36–42. https://doi.org/10.1016/J.MATDES.2012.03.048.
[6] Liu, C., Bhole, S.D., 2013, Challenges and Developments in Pipeline Weldability and Mechanical Properties. Science and Technology of Welding and Joining, 18/2: 169–181. https://doi.org/10.1179/1362171812Y.0000000090.
[7] Babu, S.S., 2011, In Pursuit of Optimum Welding System Design for Steels. Science and Technology of Welding and Joining, 16/4: 306–312. https://doi.org/10.1179/1362171811Y.0000000019.
[8] Wu, C.S., Chen, M.A., Lu, Y.F., Serindağ, H.T., Çam, G., 2021, Microstructure and Mechanical Properties of Gas Metal Arc Welded AISI 430/AISI 304 Dissimilar Stainless Steels Butt Joints. Journal of Physics: Conference Series, 1777/1:012047https://doi.org/10.1088/1742-6596/1777/1/012047.
[9] Serindağ, H.T., Tardu, C., Kirçiçek, İ.Ö., Çam, G., 2022, A Study on Microstructural and Mechanical Properties of Gas Tungsten Arc Welded Thick Cryogenic 9% Ni Alloy Steel Butt Joint. CIRP Journal of Manufacturing Science and Technology, 37:1–10. https://doi.org/10.1016/J.CIRPJ.2021.12.006.
[10] Alipooramirabad, H., Paradowska, A., Ghomashchi, R., Reid, M., 2017, Investigating the Effects of Welding Process on Residual Stresses, Microstructure and Mechanical Properties in HSLA Steel Welds. Journal of Manufacturing Processes, 28:70–81. https://doi.org/10.1016/J.JMAPRO.2017.04.030.
[11] Mao, G., et al., 2017, Effect of Nickel Contents on the Microstructure and Mechanical Properties for Low-Carbon Bainitic Weld Metals. Journal of Materials Engineering and Performance, 26/5: 2057–2071. https://doi.org/10.1007/s11665-017-2638-2.
[12] Lan, L., Kong, X., Qiu, C., Zhao, D., 2016, Influence of Microstructural Aspects on Impact Toughness of Multi-pass Submerged Arc Welded HSLA Steel Joints. Materials & Design, 90:488–498. https://doi.org/10.1016/J.MATDES.2015.10.158.
[13] Jorge, J.C.F., et al., 2019, Influence of Welding Procedure and PWHT on HSLA Steel Weld Metals. Journal of Materials Research and Technology, 8/1: 561–571. https://doi.org/10.1016/J.JMRT.2018.05.007.
[14] Ragu Nathan, S., Balasubramanian, V., Malarvizhi, S., Rao, A.G., 2015, Effect of Welding Processes on Mechanical and Microstructural Characteristics of High Strength Low Alloy Naval Grade Steel Joints. Defence Technology, 11/3: 308–317. doi: 10.1016/J.DT.2015.06.001.
[15] Mosallaee, M., Semiromi, M.T., 2021, Effect of Nickel Content on the Microstructural, Mechanical and Corrosion Behavior of E7018-G Electrode Weld Metal. Journal of Materials Engineering and Performance, 30/12: 8901–8912. https://doi.org/10.1007/s11665-021-06100-9.
[16] Yurioka, N., Suzuki, H., 1990, Hydrogen Assisted Cracking in C-Mn and Low Alloy Steel Weldments. International Materials Reviews, 35/1: 217–249. https://doi.org/10.1179/imr.1990.35.1.217.
[17] Yang, X., et al., 2021, Microstructure and Mechanical Properties of Ultralow Carbon High-strength Steel Weld Metals with Or Without Cu-Nb Addition. International Journal of Minerals, Metallurgy and Materials, 28/1: 120–130. https://doi.org/10.1007/s12613-020-2159-0.
[18] Lakshminarayanan, A.K., Shanmugam, K., Balasubramanian, V., 2009, Effect of Welding Processes on Tensile and Impact Properties, Hardness and Microstructure of AISI 409M Ferritic Stainless Joints Fabricated by Duplex Stainless Steel Filler Metal. Journal of Iron and Steel Research International, 16/5: 66–72. https://doi.org/10.1016/S1006-706X(10)60013-1.
[19] Duan, R.H., et al., 2020, Microstructure, Crystallography, and Toughness in Nugget Zone of Friction Stir Welded High-strength Pipeline Steel. Materials Science and Engineering: A, 791:139620https://doi.org/10.1016/J.MSEA.2020.139620.
[20] Balasubramanian, V., Guha, B., 2004, Effect of Welding Processes on Toe Cracking Behaviour of Pressure Vessel Grade Steel. Engineering Failure Analysis, 11/4: 575–587. https://doi.org/10.1016/J.ENGFAILANAL.2003.09.005.
[21] Byun, J.S., et al., 2001, Inoculated Acicular Ferrite Microstructure and Mechanical Properties. Materials Science and Engineering: A, 319–321:326–331. https://doi.org/10.1016/S0921-5093(00)02014-1.
[22] Ghomashchi, R., Costin, W., Kurji, R., 2015, Evolution of Weld Metal Microstructure in Shielded Metal Arc Welding of X70 HSLA Steel with Cellulosic Electrodes: A Case Study. Materials Characterization, 107:317–326. https://doi.org/10.1016/J.MATCHAR.2015.07.032.
[23] Datta, R., Mukerjee, D., Jha, S., Narasimhan, K., Veeraraghavan, R., 2002, Weldability Characteristics of Shielded Metal Arc Welded High Strength Quenched and Tempered Plates. Journal of Materials Engineering and Performance, 11/1: 5–10. https://doi.org/10.1007/s11665-002-0001-7.
[24] Lan, L., Kong, X., Qiu, C., Zhao, D., 2016, Influence of Microstructural Aspects on Impact Toughness of Multi-pass Submerged Arc Welded HSLA Steel Joints. Materials & Design, 90:488–498. https://doi.org/10.1016/J.MATDES.2015.10.158.
[25] Zhu, Z., Kuzmikova, L., Li, H., Barbaro, F., 2014, Effect of Inter-critically Reheating Temperature on Microstructure and Properties of Simulated Inter-critically Reheated Coarse Grained Heat Affected Zone in X70 Steel. Materials Science and Engineering: A, 605:8–13. https://doi.org/10.1016/J.MSEA.2014.03.034.
[26] You, Y., Shang, C., Chen, L., Subramanian, S., 2013, Investigation on the Crystallography of the Transformation Products of Reverted Austenite in Intercritically Reheated Coarse Grained Heat Affected Zone. Materials & Design, 43:485–491. https://doi.org/10.1016/J.MATDES.2012.07.015.
[27] Jung, D.-H., Kwon, J.-K., Woo, N.-S., Kim, Y.-J., Goto, M., Kim, S., 2014, S–N Fatigue and Fatigue Crack Propagation Behaviors of X80 Steel at Room and Low Temperatures. Metallurgical and Materials Transactions A, 45/2: 654–662. https://doi.org/10.1007/s11661-013-2012-4.
[28] Li, X., Zhao, J., Wang, J., Wang, X., Liu, S., Shang, C., 2020, Effect of Boundaries on Toughness in High-strength Low-alloy Steels from the View of Crystallographic Misorientation. Materials Letters, 259:126841https://doi.org/10.1016/J.MATLET.2019.126841.
[29] Hu, J., Du, L.X., Wang, J.J., Gao, C.R., 2013, Effect of Welding Heat Input on Microstructures and Toughness in Simulated CGHAZ of V–N High Strength Steel.

Materials Science and Engineering: A, 577:161–168. https://doi.org/10.1016/J.MSEA.2013.04.044.

[30] Guo, N., Liu, D., Guo, W., Li, H., Feng, J., 2015, Effect of Ni on Microstructure and Mechanical Properties of Underwater Wet Welding Joint. Materials & Design, 77:25–31. https://doi.org/10.1016/J.MATDES.2015.04.007.

[31] Lan, L., Qiu, C., Zhao, D., Gao, X., Du, L., 2012, Analysis of Microstructural Variation and Mechanical Behaviors in Submerged Arc Welded Joint of High Strength Low Carbon Bainitic Steel. Materials Science and Engineering: A, 558:592–601. https://doi.org/10.1016/J.MSEA.2012.08.057.

[32] Li, X., Fan, Y., Ma, X., Subramanian, S.V., Shang, C., 2015, Influence of Martensite–Austenite Constituents Formed at Different Intercritical Temperatures on Toughness. Materials & Design, 67:457–463. https://doi.org/10.1016/J.MATDES.2014.10.028.

[33] Haugen, V.G., Rogne, B.R.S., Akselsen, O.M., Thaulow, C., Østby, E., 2014, Local Mechanical Properties of Intercritically Reheated Coarse Grained Heat Affected Zone in Low Alloy Steel. Materials & Design, 59:135–140. https://doi.org/10.1016/J.MATDES.2014.02.010.